Formation of Nanoporous Features, Flat Surfaces, or Crystallographically Oriented Etched Profiles by the Si Chemical Dry Etching Using the Reaction of F2 + NO → F + FNO at an Eleva...

Article *in* The Journal of Physical Chemistry C · September 2013

Impact Factor: 4.77 · DOI: 10.1021/jp4084794

5 authors, including:

Satomi Tajima
Toyota Central R & D Labs., Inc.
28 PUBLICATIONS **153** CITATIONS
SEE PROFILE

Toshio Hayashi
Nagoya University
70 PUBLICATIONS **503** CITATIONS
SEE PROFILE

Kenji Ishikawa
Nagoya University
166 PUBLICATIONS **763** CITATIONS
SEE PROFILE

Makoto Sekine
Nagoya University
209 PUBLICATIONS **1,210** CITATIONS
SEE PROFILE

THE JOURNAL OF PHYSICAL CHEMISTRY C

Article

pubs.acs.org/JPCC

Formation of Nanoporous Features, Flat Surfaces, or Crystallographically Oriented Etched Profiles by the Si Chemical Dry Etching Using the Reaction of F_2 + NO → F + FNO at an Elevated Temperature

Satomi Tajima,* Toshio Hayashi, Kenji Ishikawa, Makoto Sekine, and Masaru Hori

Plasma Nanotechnology Research Center (PLANT), Graduate School of Engineering, Nagoya University, Furo-cho, Chikusa-ku, Nagoya, Aichi 464-8603, Japan

ABSTRACT: Chemical dry etching of Si was performed using the reaction of F_2 + NO → F + FNO at an elevated temperature. The etched profile, surface morphology, and surface chemical bonding structures, measured by a scanning electron microscope, X-ray photoelectron spectroscopy (XPS), and a Fourier transform infrared spectrometer (FT-IR), were significantly changed when the substrate was heated at 27 and 300 °C. Differences in total energies of Si before and after the chemical reaction with gas molecules in the etching apparatus were theoretically calculated by the density functional theory (DFT) using CAM-B3LYP/6-311G+(d,p) in Gaussian 09. The possible change in chemical bonding structures during and after the Si etching was considered by correlating the measured XPS and FT-IR spectra and the DFT calculation results. When the Si sample was heated at 27∼60 °C, the nanoporous features were observed since molecules present in the gas phase remained in the condensed layer near the Si surface and they reacted with the Si surface at different rates. The chemisorbed F_2, F, and FNO promoted Si etching by cleaving different bonds to form dangling bonds, whereas NO and OH, produced from the reaction between H_2O and F, inhibited the etching by encapsulating dangling bonds. The etch rate was significantly reduced, and the evolution of the flat surface was observed at 60∼230 °C due to the reduction of chemisorbed F_2, F, and FNO on the Si surface. When the Si sample was heated at above 230 °C, the etch rate increased with the temperature due to the amplification of the reaction rate constants of F_2, F, and FNO with the Si surface. Unique orientation-dependent etching was observed at these temperatures due to the termination of dangling bonds by F without cleaving the Si−Si lattice bonds. The contribution of NO and OH at above 230 °C was ignored since they desorbed from the Si surface.

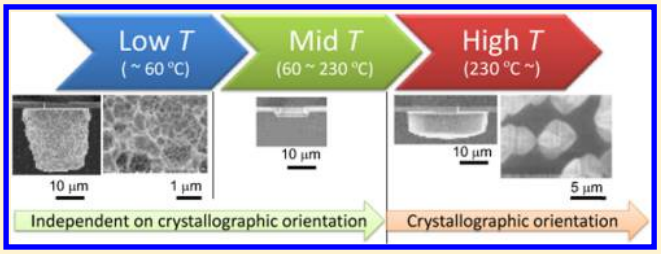

I. INTRODUCTION

Chemical dry etching of Si by various gases such as F_2,[1−4] XeF_2,[1,4,5] ClF_3,[6−10] and NO with F_2 gases with[11−14] and without[15,16] the presence of the plasma has been investigated since the late 80s. We have been studying the Si etching in NO and F_2 gases with no plasma because this method is the most economical way of selectively etch Si over SiO_2 by the reaction of F_2 + NO → F + FNO over other selections of process gases.[16] This etching technique can be used for texturing the solar panel surface to improve the light−electricity conversion efficiency,[17] removing the plasma-induced damaged layer during the gate etching process,[18] improving the device reliability by terminating dangling bonds in the gate oxide with F,[19] and eliminating the sacrificial layer to fabricate the microelectromechanical system (MEMS).[20]

In our previous study, a Si p-type (100) sample was etched at ∼5 μm/min at room temperature using the exothermic reaction of NO + F_2 → F + FNO. We conducted density functional theory calculations and found that F with the total energy of 0.8 eV can be generated by this reaction. The etch rate and the surface morphology varied significantly with the addition of NO to F_2.[16] Also, our preliminary results showed that when the substrate was heated at different temperatures, the etched profile was dramatically changed.[21] This etching phenomenon has never been reported when F_2, XeF_2, or ClF_3 was used as an etchant gas.[1−10]

In this study, we investigated the contribution of F_2, NO, F, and FNO to the Si etch rate, the etched profile, and surface morphology when the Si sample was heated at 27 and 300 °C. The etch rate, the etched profile, and the etched surface morphology were measured empirically with a scanning electron microscope (SEM), a scanning white light interferometer (SWLI), and an atomic force microscope (AFM). The changes in the surface chemical bonding structure were measured by X-ray photoelectron spectroscopy (XPS) and Fourier transform infrared spectroscopy (FT-IR). The possible chemical bonding structures were computed by the density functional theory (DFT), and the calculation results were

Received: August 24, 2013
Revised: September 5, 2013
Published: September 6, 2013

   dx.doi.org/10.1021/jp4084794 | J. Phys. Chem. C 2013, 117, 20810−20818

compared to the XPS and FT-IR spectra to elucidate the cause of the dramatic change in etched profile when the Si was heated at different temperatures.

II. EXPERIMENTAL PROCEDURES

Process Chamber. A Si etching apparatus used in this study was described elsewhere.[16] The base pressure of this chamber was maintained at ~10^{-1} Pa by the dry pump so that the small amount of H_2O is considered to be present in the chamber. A 6 mm (width) × 15 mm (length) × 0.53 mm (thickness) Si sample was placed on the ceramic heater which was covered by the Al foil inserted in the Pyrex tube with the inner diameter of 25 mm and the length of 150 mm. The Si sample was exposed to the gas mixture of NO at a flow rate of 5 sccm (8.5×10^{-3} Pa m^3/s) diluted with Ar at a flow rate of 49.5 sccm (8.4×10^{-2} Pa m^3/s) and Ar/5% F_2 at a flow rate of 54.5 sccm (9.2×10^{-2} Pa m^3/s). The corresponding F_2 flow rate was 2.7 sccm (4.6×10^{-3} Pa m^3/s). In this study, the temperature on the ceramic heater was adjusted between 27 and 300 °C by the variable autotransformer while measuring the temperature by the K-type thermocouple placed on top of the ceramic heater under the Si substrate. Pressure in the Pyrex tube was maintained at 600 Pa throughout the process time of 0.5 and 5 min.

Materials. Two Si samples were prepared. One was a p-type Si(100) sample with the resistivity of ~1000 Ω cm with a 1 μm thick SiO_2 mask layer which was fabricated by the plasma-enhanced chemical vapor deposition (PECVD) of tetraethyl orthosilicate (TEOS $Si(OC_2H_5)_4$) that had 8 μm × 8 μm square patterns. This sample was exposed to NO and F_2 gases for 5 min for the etch rate and the etched profile analysis. The other was the nondoped Si(100) sample with the resistivity of >3000 Ω cm for the surface morphology and the surface chemical bonding structure analysis. This sample was cleaned with acetone, ethanol, deionized (DI) water, 13% hydrochloric acid, and 49% hydrofluoric (HF) acid for 5 min, followed by rinsing in DI water for <5 s to terminate the Si surface with H. This H-terminated Si sample was exposed to NO and F_2 gases for 0.5 min in the aforementioned process chamber.

Analysis Methods. The etch rate, the etched profile, and the surface morphology of the patterned p-type Si were observed by the SEM (S-5200 Hitachi High-Technologies Corporation, Tokyo, Japan) with an acceleration voltage of 2 kV and the magnification of ×3000−30 000. The root-mean-square (rms) roughness from the 10 μm × 10 μm scan area of the nondoped Si surface were measured by the SWLI with ×50 objective lens (Zygo, New View TM 6200, Zygo Co., Middlefield, CT, USA) and the AFM (DI-2100 Veeco Instruments Inc. Plainview, NY, USA). The etched depth, d [μm], the vertical etched length, δ [μm], mask openings, w_m [μm], and maximum width under the mask, w, which was the sum of w_m [μm] and 2δ [μm], were measured from eight different etched patterns from multiple samples. The vertical etch rate E_V [μm/min] and the lateral etch rate E_L [μm/min] were calculated by d [μm] and δ [μm] divided by the etched time of 5 min, respectively. Aspect ratio, a_h, was determined by taking the ratio of E_V and E_L. Anisotropy requirement was evaluated by the following equation from the etched geometries.[22]

$$a_h = E_V/E_L = d/\delta \geq 2d/(w - w_m) \quad (1)$$

Changes in surface chemical bonding structures before and after the etching in NO and F_2 gases at different temperatures were analyzed by XPS (Escalab 220i-XL, VG scientific, Currently under Thermofisher, Waltham, MA, USA) and FT-IR (Nicolet 8700, Thermo Fisher Scientific, Waltham, MA). The nondoped Si samples were etched in NO and F_2 gases within 5 h after the sample cleaning, and they were placed in the XPS loading chamber, which was maintained at less than 10^{-6} Pa, within 60 min after the etching. XPS spectra with a Mg Kα (E = 1253.6 eV) source were taken from the 5 mm^2 sampling area with an electron takeoff angle of 90°. Survey spectra were collected with the pass energy of 187 eV with the resolution of 1.0 eV. The high-resolution scans were obtained by adjusting the pass energy of 50 eV for C 1s and Si 2p and 20 eV for O 1s, F 1s, and N 1s with the resolution of 0.05 eV. The highest peak position of the C 1s core level, which was incorporated by the physisorption of the contaminant during the sample transfer between rinsing, etching, and XPS analysis, was adjusted at 285 eV to compensate the surface charging. After the background was subtracted by the Touggard method,[23] all spectra were fitted with 80% Gaussian−20% Lorentzian distributions using the XPS spectra analysis software (XPSPEAK 4.1). The atom fraction of Si, F, N, and O in the sample can be calculated as follows.[24,25]

$$\text{Atom fraction of element X (Si, F, N, or O)} = \frac{n_x}{\sum n_x} = \frac{I_x/S_x}{\sum I_i/S_i} \quad (2)$$

$$n = \frac{I}{f\sigma\theta y\lambda AT} = I/S \quad (3)$$

where I is the number of photoelectrons per second in a specific spectra peak; n is the number of atoms of the element per cm^3 of the sample; f is the X-ray flux [photons/cm^2 s]; σ is the photoelectric cross-section for the atomic orbital of interest [cm^2]; θ is an angular efficiency factor for the instrumental arrangement based on the angle between the photon path and detected electron; y is the efficiency in the photoelectric process for formation of photoelectrons of the normal photoelectron energy; λ is the mean free path of the photoelectrons in the sample; A is the area of the sample from which photoelectrons are detected; T is the detection efficiency electrons emitted from the sample; and S is the atomic sensitivity factor. S of Si, F, N, and O is 0.296, 1.000, 0.477, and 0.711, respectively.[24,25]

Infrared absorption spectra from the Si samples exposed to NO and F_2 gases were measured by transmission FT-IR with the scan number of 128 and the resolution of 4 cm^{-1}. The FT-IR measurement of the background spectra of untreated sample was performed within 5 h after the sample cleaning, and the absorption spectra were taken from the Si surface within 10 min after the completion of the etching process.

III. THEORETICAL CALCULATIONS

Surface Reaction during the Etching. Not only F_2, NO, F, and FNO but H_2O were considered to be present in the process chamber since the base pressure was in the range of 10^{-1} Pa. Only F may react with H_2O to produce HF and OH exothermically. OH may be desorbed from the SiO_2 mask fabricated by the PECVD. Changes in total energies and the chemical bonding structures of Si reacted with F_2, NO, F, FNO, H_2O, HF, and OH were calculated by the DFT. The Si(100)-2 × 1 cluster model was used to describe the top four layers of the Si lattice. From our previous study, only F and Si_9H_{14} reacted exothermically to form HF and Si_9H_{13} with one

dx.doi.org/10.1021/jp4084794 | J. Phys. Chem. C 2013, 117, 20810−20818

dangling bond.[16] At least one dangling bond at the Si surface was necessary to initiate the reaction with F_2, NO, F, and/or FNO. Therefore, we incorporated two Si surface models with different number of dangling bonds in this study, i.e., Si_9H_{13} with one H-termination and one dangling bond at the surface and Si_9H_{12} with two dangling bonds at the surface. Geometries of F_2, NO, F, FNO, H_2O, HF, and/or OH + Si_9H_{12} or Si_9H_{13} were optimized, and minimum total energies before and after the chemical reaction were computed by CAM-B3LYP/6-311G +(d,p) in Gaussian 09, where CAM-B3LYP could integrate the long-range correction such as the polarizability of long chains, excitations of Rydberg states, and charge transfer excitations.[26]

IV. RESULTS AND DISCUSSION

Etched Profile and Surface Morphology. Figure 1 shows the representative cross-sectional SEM images of the patterned p-type Si(100) samples placed in NO and F_2 gases when the Si was heated at 27~300 °C. E_V, E_L, d, δ, w_m, and w were measured from SEM images to evaluate the anisotropic requirement based on eq 1. From the measurement, we found that the Si was anisotropically etched in NO and F_2 gases when the substrate was heated at 27~300 °C. The E_V, E_L, and a_h are plotted with respect to the 1000/T [K^{-1}] in Figure 2.

When the heater temperature was ramped from 27 to 60 °C, the a_h was 3.5 at 27 °C and sharply reduced to ~1 at 60 °C. The E_V, the E_L, and the roughness decreased with the temperature. Nanoporous features were observed in the microscopically rough etched profile shown in Figure 1(a)(I) at this temperature range. The mechanism of the generation of the rough etched profile was discussed in our previous study in detail.[16] When the Si sample was heated at 60~230 °C, the a_h remained 1, and the etched bottom surface became smooth with the absence of nanoporous features (Figure 1(a)(II)). Both the E_V and the E_L decreased with the increase of the temperatures up to ~70 °C, and they increased again at temperatures above 70 °C (see Figure 2). The E_V and the E_L at ~70 °C were 1 order of magnitude smaller than that at 27 °C. When the heater was adjusted at above 230 °C, the sidewall of the etched profile became vertical as shown in Figure 1(a)(III). The magnified view of the corner and the bottom of the etched Si profile at 300 °C were listed in Figure 1(b). The crystallographic orientation was observed from these SEM images where the bottom surface was {100} and the sidewall was {110}. Corner undercutting[27] with the exposure of {211} and {411} was also observed at the corner of the etched profile.

The morphology of the etched bottom surface and the sidewall surface of the p-doped Si was dramatically changed when the Si was heated at different temperatures as shown in Figure 1. Figure 3 shows the top view of the H-terminated nondoped Si(100) placed in the NO and F_2 gases for 0.5 min while adjusting the temperature at 27 and 230 °C. The rms roughness of nondoped Si etched for 0.5 min was 122.4 nm at 27 °C (measured by SWLI), 0.5 nm (measured by AFM) at 60 °C, and 2.4 nm (measured by AFM) at 300 °C. The Si surface etched in NO and F_2 gases at 27 °C had three different sizes of etch pits with diameters of 50−100 nm, 300−600 nm, and 2−5 μm, and they were marked as A, B, and C in Figure 3(a), respectively. Neither nanoporous features nor microscale etch pits were observed by SEM and AFM when the Si was etched at 60~230 °C. The Si surface exposed to NO and F_2 gases at above 230 °C had square patterns as shown in Figure 3(b) with the appearance of {211}, confirming that the etch rate was different with the crystallographic orientation as shown in Figure 1(b).

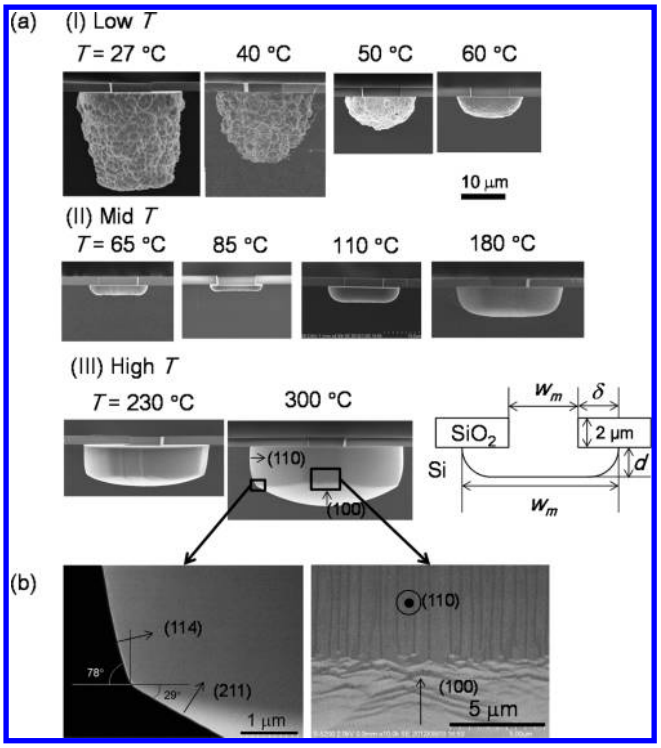

Figure 1. (a) Cross-sectional SEM images of p-type Si(100) with SiO_2 mask with 8 μm × 8 μm square openings etched in NO and F_2 gases with flow rates of NO, Ar, and Ar/5% F_2 at 5, 49.5, and 54.5 sccm, respectively. The chamber pressure was maintained at 600 Pa throughout the process time of 5 min. The Si sample was heated at 27~300 °C. (I) The rough etched surface observed at 27−60 °C, (II) the flat etched surface observed at 65−180 °C, and (III) the orientation-dependent etched surface observed at 230−300 °C. (b) The magnified view of the corner, the sidewall, and the bottom of the etched surfaces at 300 °C.

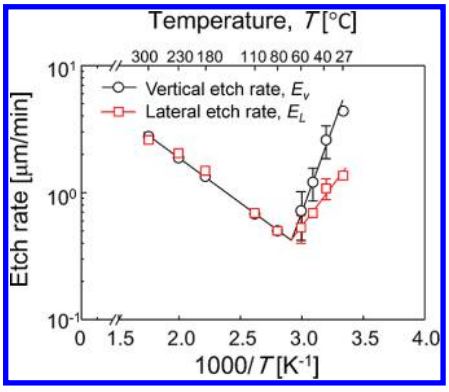

Figure 2. Relationship between the vertical etch rate, E_V, the lateral etch rate, E_L, the aspect ratio, a_h, and the inverse of the applied temperature, 1000/T [K]. The patterned p-type Si(100) was used to evaluate E_V, E_L, and a_h. The etching was performed in the mixture of NO, Ar, and Ar/5% F_2 at the flow rates of 5, 49.5, and 54.5 sccm, respectively. The chamber pressure was maintained at 600 Pa during the process time of 5 min while heating the Si sample at 27~300 °C.

The microscopically rough etched profile depicted in Figure 1(a)(I) and Figure 3(a) and the etch rate curve shown in Figure 2 were observed when the Si was chemically dry etched in XeF_2 or ClF_3 gases.[3,4] Previous studies stated that the

dx.doi.org/10.1021/jp4084794 | J. Phys. Chem. C 2013, 117, 20810−20818

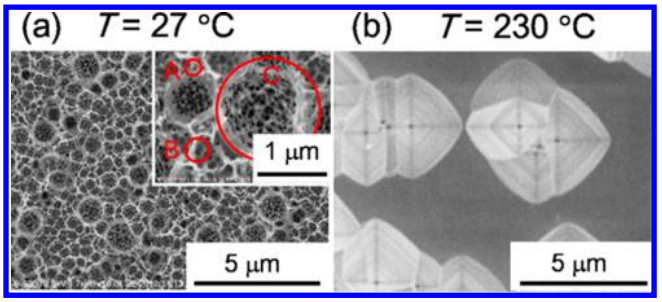

Figure 3. SEM images of the nondoped Si(100) sample that was etched in NO and F_2 gases while heating the Si sample at (a) 27 °C and (b) 230 °C. The flow rates of NO, Ar, and Ar/5% F_2 were 5, 49.5, and 54.5 sccm, respectively. The chamber pressure was maintained at 600 Pa during the process time of 0.5 min.

evolution of the rough surface was due to the chemisorption of not only F but also XeF_2, XeF, ClF_3, Cl_2, and Cl that would etch Si differently.[28,29] The residence time of those molecules on the Si surface was long when the substrate temperature was low. The fast Si etch rate at the low temperature in NO and F_2 gases observed in Figures 1 and 2 can be explained by the presence of the chemisorbed F_2 and F that would promote the etching. In addition to F_2 and F, NO would inhibit the etching by capping the dangling bonds. FNO would act as both a promoter and an inhibitor of the Si etching process by producing and capping the dangling bonds at the surface. The initiation and the capping of dangling bonds from different layers of the Si lattice at different rate constants lead to the formation of various sizes of etch pits.[16]

These multiple reactions between molecules in the gas phase and the Si surface not only induced a microscopically rough etched profile but also produced complex nanoporous features at low temperature.

When the Si sample was heated at above 60 °C, the etched surface became smooth, and the etch rate reduced dramatically as shown in Figure 1(a)(II) and Figure 2. The significant decrease of the etch rate and the formation of the smooth surface at 60∼230 °C were considered to be due to the reduction of chemisorbed F_2, F, and FNO, acting as an etching promoter at the proximity of the Si surface. The orientation-dependent etching was observed only when the Si sample was heated at above 230 °C. To elucidate why this significant change in etched profile was observed by the relatively small variation of the heat applied to the Si sample, surface chemical bonding structures were analyzed in the subsequent sections.

Surface Chemical Bonding Structures. Figure 4(a) shows the XPS survey spectra from the nondoped Si before and after the etching in NO and F_2 gases for 0.5 s at 27∼300 °C. The C was physisorbed on the Si surface as a contaminant during the sample transfer in the air between rinsing, etching, and XPS analysis, and they did not react with Si, F, and/or F_2. This was confirmed by the absence of the Si−C peak at 284.2 eV,[30] CF_2 peak at 291.5 eV, and CF_3 peak at 293.5 eV.[31,32]

The atom fraction of N was 0.5−1% at all conditions, and those values were independent of the applied temperature. Figure 4(b) shows the XPS Si 2p spectra from the Si surface before and after the etching in NO and F_2 gases when the substrate was heated at 27∼300 °C. The relative area ratios of $Si-Si_4$ (marked as (i)), silicon suboxyfluoride ($Si-SiO_xF_y$ ($x \leq$

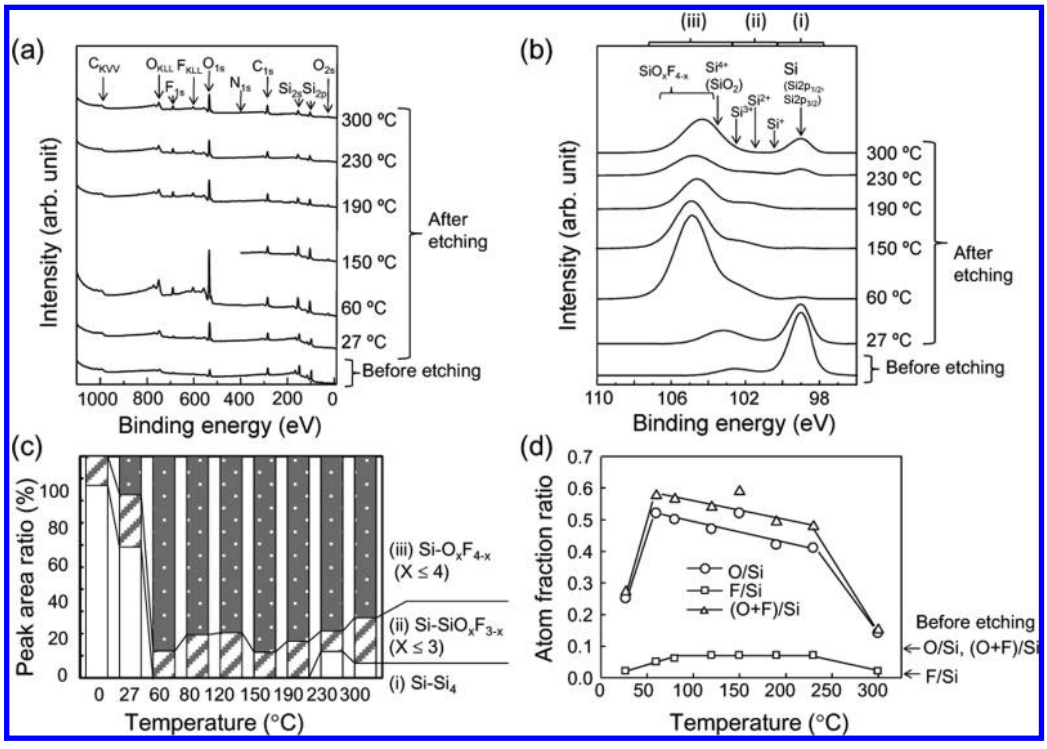

Figure 4. (a) XPS survey spectra and (b) Si 2p high-resolution spectra from the nondoped Si(100) sample before and after the etching in NO and F_2 gases. (c) The relative area ratio of $Si-Si_4$, silicon suboxyfluoride ($Si-SiO_xF_y$ ($x \leq 3$)), and silicon oxyfluoride (SiO_xF_{4-x} ($x \leq 4$)) measured after the peak fitting of the Si 2p XPS spectra shown in (b). (d) Atom fraction ratio of O/Si, F/Si, and (O + F)/Si calculated from Si 2p, O 1s, and F 1s high-resolution XPS spectra taken from the nondoped Si(100) sample etched in NO and F_2 gases. The etching was performed with flow rates of NO, Ar, and Ar/5% F_2 of 5, 49.5, and 54.5 sccm, respectively. The chamber pressure was maintained at 600 Pa during the process time of 0.5 min while heating the Si sample at 27∼300 °C.

dx.doi.org/10.1021/jp4084794 | J. Phys. Chem. C 2013, 117, 20810−20818

3)) (marked as (ii)), and silicon oxyfluoride (SiO_xF_{4-x} ($x \leq 3$)) (marked as (iii)) were measured from the peak-fitted Si 2p spectra, and the results are summarized in Figure 4(c).

Si $2p_{3/2}$ plus Si $2p_{1/2}$ from the Si matrix (Si−Si_4)[33] at the maximum peak position of 99 eV with the full width at half-maximum (fwhm) of 1.2 eV and Si suboxide at the maximum peak position of 102 eV with the fwhm of 2 eV were present after the Si sample was rinsed and terminated by H. This suboxide was formed when the sample was exposed to the air between rinsing and XPS analysis. After the Si was placed in NO and F_2 gases at 27 °C, multiple peaks were evolved at the peak position in the range of 100−104 eV. These peaks are from suboxide and/or suboxyfluoride (Si^+ at 100.4 eV (Si_2O and/or Si−$Si_3O_xF_{1-x}$ ($x \leq 1$)), Si^{2+} at 101.4 eV (SiO and/or Si−$Si_2O_xF_{2-x}$ ($x \leq 2$)), Si^{3+} at 102.4 eV (Si_2O_3 and/or Si-SiO_xF_{3-x} ($x \leq 3$))). The peak at 103.4 eV was Si^{4+} at 103.4 eV (SiO_2 and/or Si−O_3F).[33,34] When the Si sample was heated at above 60 °C, the Si matrix peak at the peak position of 99 eV and Si^+ peak at 100.4 eV significantly reduced. Instead, the peak at >104 eV with the fwhm of >2 eV evolved, which can be assigned as Si−O_xF_{4-x} ($x \leq 4$). When the Si sample was heated at above 230 °C, the Si matrix peak reappeared at 99 eV, and this peak intensity increased with the temperature. Multiple peaks were observed from O 1s and F 1s spectra, indicating the presence of silicon oxyfluoride with different stoichiometry.

An atom fraction of Si, O, F, and N was calculated from the area under the peak of Si 2p, O 1s, F 1s, and N 1s using eq 2 with the aforementioned atomic sensitivity factors. The atom fraction of O/Si, F/Si, and (O + F)/Si are plotted in Figure 4(d). Before etching, O/Si, F/O, and (O + F)/Si were 0.09, 0.01, and 0.099, respectively. When the Si was etched in NO and F_2 gases at 27 °C, O/Si, F/O, and (O + F)/Si became 0.25, 0.02, and 0.27, respectively. When the Si was etched at above 60 °C, O/Si, F/O, and (O + F)/Si became 0.52, 0.05, and 0.57, respectively. O/F and (O + F)/Si gradually decreased with temperatures up to 230 °C, whereas F/Si remained the same at 0.07. O/Si, F/Si, and (O + F)/Si dramatically reduced to 0.14, 0.02, and 0.15 when the Si was etched at 300 °C.

The change in O/Si, F/O, and (O + F)/Si with respect to the applied temperature shown in Figure 4(d) matched well with the Si 2p peak area ratio summarized in Figure 4(c) where Si−Si_4 and Si suboxyfluride were present at the surface of Si that was etched below 60 °C (O + F/Si < 0.5) and the complete coverage of the silicon oxyfluoride layer on the Si surface at 60−230 °C (O + F/Si > 0.5), and the reduction of Si oxyfluoride and the increase of the Si−Si^4 at the surface of Si etched were observed at above 230 °C.

Figure 5 shows the FT-IR absorption bands from the nondoped Si sample that was etched for 0.5 min in NO and F_2 gases when the Si sample was heated at 27, 60, 80, 230, and 300 °C. Four broad bands were observed in the range of 743−841 cm^{-1} (Si−O bending),[35] 860−1013 cm^{-1} (Si−F stretching),[36] 1013−1130 cm^{-1} (Si−O in-phase stretching),[37,38] and 1130−1311 cm^{-1} (Si−O out-of-phase stretching)[37] from the etched Si samples. All peak intensities were initially low when the Si was etched at 27 °C, and they became high at 60∼230 °C and reduced at above 230 °C. FT-IR results indicated that the large amount of Si−O and Si−F bonds existed at the Si surface when the substrate was heated at 60∼230 °C. The number of those bonds became low when the Si sample was heated to less than 60 °C and more than 230 °C. The change in the number of S−O and Si−F bonds at the surface was correlated well with O/Si and F/Si ratio with respect to the applied temperature

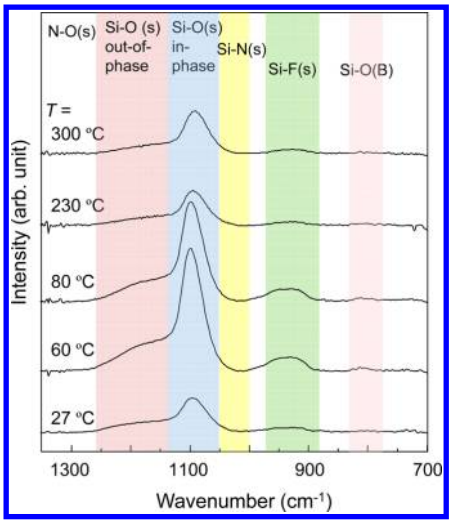

Figure 5. FT-IR absorption spectra obtained from the nondoped Si(100) sample etched in NO and F_2 gases. The flow rates of NO, Ar, and Ar/5% F_2 were 5, 49.5, and 54.5 sccm, respectively. The chamber pressure was maintained at 600 Pa during the process time of 0.5 min while heating the Si sample at 27∼300 °C.

measured by XPS as shown in Figure 4(d). Si−N stretching (820−840 cm^{-1})[39] and Si−(O, N) stretching (900−1000 cm^{-1})[40] overlap Si−O bending and Si−O stretching, so it was difficult to distinguish the presence of N from these peaks. However, the absence of N−O stretching at >1311 cm^{-1}[41] suggested that a very small amount of NO was present at the Si surface. This result matched well with the low atom fraction of N from the XPS results shown in Figure 4(a).

The change in total energies before and after the chemical reaction between Si_9H_x (X = 12 or 13) and F_2, NO, F, FNO, H_2O, OH, and HF was calculated by B3LYP/CAM6-311G+(d, p) in Gaussian 09 to identify whether those chemical reactions are exothermic or endothermic, and the results are summarized in Table 1. The reaction between H_2O or HF and Si_9H_x (x = 12, 13) was endothermic and must overcome the energies of more than 2.0 eV for the reaction. Therefore, the reaction of Si_9H_x + H_2O or Si_9H_x + HF would not happen at the process conditions in this study. H_2O or HF would not react with the Si surface that was terminated by F ($Si_9H_{12}F_2$) either. The bond energy between Si_9H_x and F_2 was the highest, followed by those between Si_9H_x and F, OH, FNO, and NO. The bond energy between Si_9H_x and NO was 0.8∼0.9 eV so that NO can be

Table 1. Difference in Bond Energies before and after the Reaction between Atoms and Molecules Present in the Gas Phase and Si_9H_x (x = 12 and 13)[a]

	difference in bond energies before and after the reaction (eV)	
	Si surface model Si_9H_{13}	Si surface model Si_9H_{12}
F_2	−7.7	−9.9
NO	−0.9	−0.8
F	−5.7	−5.6
FNO	−4.4	−4.0
OH	−4.6	−4.5
HF	endothermic	endothermic
H_2O	endothermic	endothermic

[a]The calculation was performed by CAM-B3LYP/6-311G+(d,p) in Gaussian 09.

dx.doi.org/10.1021/jp4084794 | J. Phys. Chem. C 2013, 117, 20810−20818

easily desorbed from the surface when the Si lattice vibration increased at an elevated temperature. The chemical reaction between OH and Si was considered to be low at the high temperature since most of the H_2O was eliminated from the Si surface and very little OH was produced.

Figure 6 shows the optimized chemical bonding structure that had minimum total energies after the reaction between Si_9H_x and F_2, F, OH, FNO, and NO. F abstraction occurs differently when F_2 reacted with the Si that had either one or two dangling bonds. When the Si_9H_{13} reacted with F_2, both the

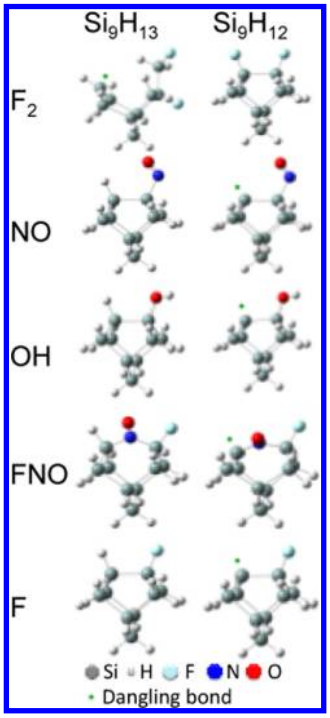

Figure 6. Calculated chemical bonding structures of Si_9H_x (x = 12 and 13) after the reaction with F_2, NO, F, FNO, and OH. These structures were determined by CAM-B3LYP/6-311G+(d,p) in Gaussian 09.

Si−Si σ-dimer and Si−Si σ-lattice bonds were cleaved, and F was abstracted from F_2. When the Si_9H_{12} reacted with F_2, F was abstracted and reacted with two dangling bonds at the Si surface. F abstraction from the reaction between the F_2 and Si surface with the dangling bonds was empirically observed in previous studies.[42−44] When the FNO approached to the Si_9H_x surface, F reacted with the dangling bond, and NO was placed in the middle of the Si−Si σ-dimer bonds. During the cleavage of the Si−Si σ-dimer bonds, new dangling bonds were formed at the Si surface.[16] F, OH, and NO terminated the dangling bond at the Si surface, and no Si−Si σ-dimer bond or Si−Si σ-lattice bond cleavage was observed.

The formation of the etched profile at 27 °C with E_V/E_L ratio of ~3.5 shown in Figure 1(a)(I) has never been observed when the Si was chemically dry etched in XeF_2 or ClF_3 gases. This etched profile was produced probably due to the chemisorption of different gas molecules in the condensed layer. When the substrate temperature is low, the condensed layer may be formed at the proximity of the Si surface, and this layer plays a significant role in determining the etch rate. The condensed layer consists of not only F_2, NO, F, FNO, H_2O, HF, and/or OH but also the product of the SiF_4 with those gas molecules. When we calculate the possible chemical reaction in the condensed layer by CAM-B3LYP/6-311G+(d,p) in Gaussian 09, SiF_4 may react exothermically with HF, FNO, and OH by forming fluorosilicic acid (H_2SiF_6) and $(SiF_4)(FNO)_2$ and $(SiF_4)(OH)$. H_2SiF_6, $(SiF_4)(FNO)_2$, and $(SiF_4)(OH)$ transported from the bottom etched wall to the sidewall. H_2SiF_6 reacts with H_2O present in the chamber that could form the etch stop silicon oxyfluoride layer at the sidewall.[45] Chemisorption of H_2SiF_6 is sensitive to the change in the temperature since the melting point of H_2SiF_6 is 19 °C.[46] Two FNO molecules weakly bonded to SiF_4 to exothermically form $(SiF_4)(FNO)_2$ with their intermolecular force of 0.37 eV. This intermolecular force is larger than the hydrogen bond energy of water (~0.2 eV). Therefore, $(SiF_4)(FNO)_2$ may adsorb on the etched Si surface at a low temperature, leading to the formation of a unique anisotropic etched profile. The contribution of H_2SiF_6 and/or $(SiF_4)(FNO)_2$ to prevent sidewall etching at a low temperature still needs further investigation by utilizing in-situ gas and surface analysis techniques.

Figure 7 shows the proposed model of the different chemical reaction during the Si etching in NO and F_2 gases at different temperatures based on the XPS, FT-IR, and DFT calculation results. The Si surface can be etched by F, F_2, and FNO, while the etching was terminated by the encapsulation of the dangling bonds by OH, NO, and FNO at a low temperature. Due to the presence of those molecules near the Si surface, the etch rate varies, and this leads to the formation of nanoporous features in the microscale etch pits. Dangling bonds are formed not only at the on-top site of Si by the reaction with F but also at the inside of the Si lattice by cleaving Si−Si σ-dimer bonds and Si−Si σ-lattice bonds by the reaction with F_2 and FNO. Various molecules in the condensed layer may react with these dangling bonds at different rates.

When the Si was etched at the intermediate temperature, the chemisorbed layer consisting of F_2, NO, F, FNO, and OH as well as the product of SiF_4 and those molecules decreased, and this leads to the significant reduction of the etch rate. F_2, F, FNO, OH, and NO may react with the dangling bonds located at the on-top site of the Si and inside the Si lattice, but unreacted dangling bonds remained even after the etching in NO and F_2 at this temperature. These dangling bonds react with O_2 in the air to form a complex silicon oxyfluoride layer with different stoichiometry.

When the Si was heated at above 230 °C, the etch rate increased with the temperature due to the increase of the rate constant between the reaction of F, F_2, and FNO at the Si surface. The etching inhibitor, NO and OH, can be ignored at this temperature since NO with the low bond energy may easily desorb by the increase of the Si lattice vibration, and the contribution of OH can be ignored since the H_2O adsorption on the Si surface was low. The etching continued mainly by F from the gas phase and from the surface reaction between F_2 and the dangling bond located at the on-top site of Si. The incorporation of the high density F on the Si surface resulted in the formation of SiF_4 that would leave $Si−Si_4$ at the surface. The contribution of FNO to the Si etching was not clear at this temperature with the absence of N on the Si surface from XPS and FT-IR results. However, we still consider that the N from FNO may play a significant role in crystallographically oriented etching since the crystallographic orientation dependency was also observed by the chemical dry etching of Si with ClF_3 and N_2 gases.[47] N may be desorbed during the post-etching reaction between the Si surface with the dangling bonds and FNO and O_2 in the air. Further investigation is necessary using an in-situ

dx.doi.org/10.1021/jp4084794 | J. Phys. Chem. C 2013, 117, 20810−20818

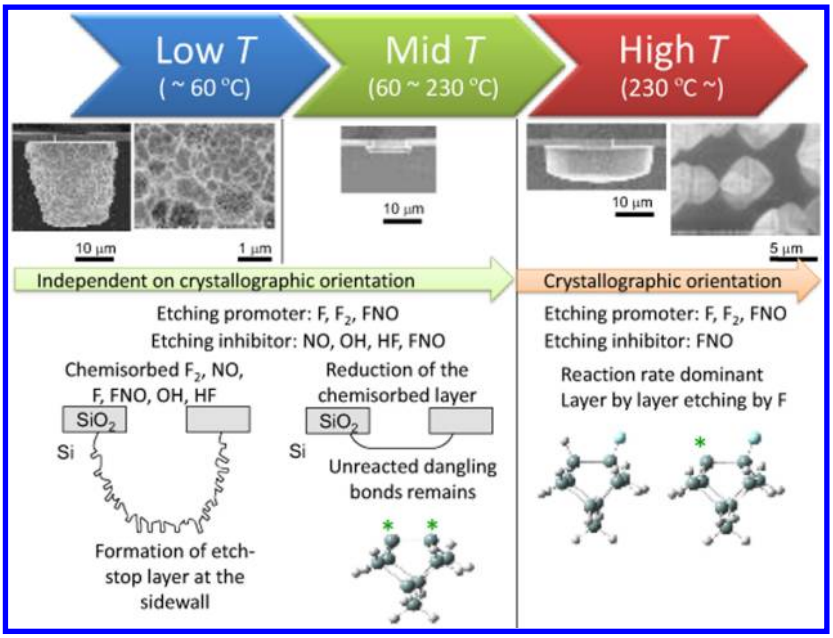

Figure 7. Proposed surface reaction model during the chemical dry etching of Si in NO and F_2 gases at three different temperature ranges.

chemical analysis technique to elucidate the contribution of N to the orientation-dependent etching.

In this study, we performed Si etching in NO and F_2 gases and produced the wide variety of etched profiles by just changing the temperature of the Si sample. Coexistence of the etching promoter, F_2, F, and FNO, and the etching inhibitor, NO, FNO, and OH, produced a rough etched profile with nanoporous features at the low temperature. The roughness can be controlled by adjusting the residence time of those molecules at the proximity of the Si surface. When the temperature was increased, the contribution of etching inhibitors, NO and OH, can be ignored, and etching was mainly proceeded by the reaction between F and Si. Since no special equipment, such as a power supply or a magnet, was necessary to produce completely different etching profiles, this chemical dry etching technique has a potential for texturing the Si surface, conducting smooth and slow etching, and producing orientation-dependent etched profiles for various applications such as the solar panel fabrication, the damage layer removal around the gate oxide, and the MEMS fabrication.

V. CONCLUSIONS

Si chemical dry etching was performed in NO and F_2 gases using the exothermic reaction of $F_2 + NO \rightarrow F + FNO$. The formation of nanoporous features, the initiation of the flat surface, or the crystallographically orientation-dependent etched profile were observed by controlling the temperature of the Si sample between 27 and 300 °C. The etched profile and the change in surface chemical bonding structures were observed by the SEM, XPS, and FT-IR. Reactions between the Si surface and F_2, NO, F, and FNO, OH, HF, and H_2O were evaluated by the DFT by assuming the different numbers of dangling bonds at the outermost layer of the Si(100)-2 × 1 cluster model. By comparing the empirical and calculation results, the chemisorbed F_2, F, and FNO promoted the Si etching by forming new dangling bonds, while NO, OH, and FNO inhibited etching by terminating the dangling bond at the Si surface at low temperatures. The multiple chemical reactions between the molecules in the gas phase and the Si surface occurred at different rates, leading to the formation of complex nanoporous features in microscopically rough etched profiles as well as the anisotropic etched profile. The reduction of chemisorbed F_2, F, and FNO decelerated the etch rate at an intermediate temperature, and the unreacted dangling bonds remained on the Si surface. When the substrate temperature was ramped at above 230 °C, the Si etching was mainly performed by F, F_2, and FNO at the Si surface, and the contribution of NO and OH could be ignored. The crystallographic orientation was evolved, and the etch rate increased with the temperature by the increase of the rate constant of F_2, F, and FNO and the Si surface.

AUTHOR INFORMATION

Corresponding Author

*Tel. & Fax: +81-52-788-6077. E-mail: stajima@plasma.engg.nagoya-u.ac.jp.

Notes

The authors declare no competing financial interest.

ACKNOWLEDGMENTS

The authors greatly acknowledge the research support funding provided by Tatematsu Zaidan, Aichi, Japan. NO gas was kindly donated from Sumitomo Seika Chemicals Co, Ltd.

REFERENCES

(1) Coburn, J. W.; Winters, H. F. Ion and Electronassisted Gassurface Chemistry—An Important Effect in Plasma Etching. *J. Appl. Phys.* **1979**, *50*, 3189–3195.

(2) Mucha, J. A.; Donnelly, V. M.; Flamm, D. L.; Webb, L. M. Chemiluminescence and the Reaction of Molecular Fluorine with Silicon. *J. Phys. Chem.* **1981**, *85*, 3529–3532.

(3) Ibbotson, D. E.; Flamm, D. M.; Mucha, J. A.; Donnelly, V. M. Comparison of XeF_2 and F atom Reactions with Si and SiO_2. *Appl. Phys. Lett.* **1984**, *44*, 1129–1131.

(4) Holt, J. R.; Hefty, R. C.; Tate, M. R.; Ceyer, S. T. Comparison of the Interactions of XeF_2 and F_2 with Si (100)(2 × 1). *J. Phys. Chem. B* **2002**, *106*, 8399–8406.

(5) Aliev, V. S.; Kruchinin, V. N. Development of Si(100) Surface Roughness at the Initial Stage of Etching in F_2 and XeF_2 Gases: Ellipsometric Study. *Surf. Sci.* **1999**, *442*, 206−214.
(6) Ibbotson, D. E.; Mucha, J. A.; Flamm, D. L.; Cook, J. M. Plasmaless Dry Etching of Silicon with Fluorinecontaining Compounds. *J. Appl. Phys.* **1984**, *56*, 2939−2942.
(7) Saito, Y.; Yamaoka, O.; Yoshida, A. Plasmaless Etching of Silicon using Chlorine Trifluoride. *J. Vac. Sci. Technol., B* **1991**, *9*, 2503−2506.
(8) Höchst, A.; Fischer, F.; Kirbach, G.; Urban, A.; Becker, V.; Irmscher, M.; Sailer, H.; Kern, D. P. Investigations on the Mechanism of Silicon Etching with Chlorine-Trifluoride. *J. Vac. Sci. Technol., B* **2005**, *23*, 1936−1942.
(9) Saito, Y. Characteristics of Plasmaless Dry Etching of Silicon-Related Materials using Chlorine Trifluoride Gas. *Sens. Mater.* **2002**, *14*, 231−237.
(10) Seki, T.; Yoshino, T.; Senoo, T.; Koike, K.; Nomnimiya, S.; Aoki, T.; Matsuo, J. High Speed Si Etching with ClF_3 Cluster Injection. *AIP Conf. Proc.* **2010**, *1321*, 317−320.
(11) Yun, Y. B.; Kim, D. J.; Park, S. M.; Lee, N.-E.; Kim, K. S.; Bae, G. H. Large Etch Rate Enhancement by NO-Induced Surface Chemical Reaction during Chemical Dry Etching of Silicon Oxide in F_2 Remote Plasmas. *J. Electrochem. Soc.* **2007**, *154*, D267−D272.
(12) Yun, Y. B.; Park, S. M.; Lee, N. -E. Effect of Plasma Modulation on Si Chemical Dry Etching in F_2 Remote Plasmas. *J. Korean Phys. Soc.* **2008**, *53*, 2386−2390.
(13) Heo, W.; Lee, N. -E. Effect of Additive N_2 and Ar Gases on Surface Smoothening and Fracture Strength of Si Wafers during High-Speed Chemical Dry Thinning. *Microelectro. Reliab.* **2012**, *52*, 412−417.
(14) Heo, W.; Ahn, J. H.; Lee, N. -E. Control of Surface Roughness during High-Speed Chemical Dry Thinning of Silicon Wafer. *J. Vac. Sci. Technol., A* **2010**, *28*, 1073−1077.
(15) Shigemoto, T.; Sonobe, J. Thermal Cleaning of Silicon Nitride with Fluorine and Additive Mixture. *ECS Trans.* **2007**, *11*, 47−54.
(16) Tajima, S.; Hayashi, T.; Ishikawa, K.; Sekine, M.; Hori, M. Room-Temperature Si Etching in NO/F_2 Gases and the Investigation of Surface Reaction Mechanisms. *J. Phys. Chem. C* **2013**, *117*, 5118−5125.
(17) Koynov, S.; Brandt, M. S.; Stutzmann, M. Black Nonreflecting Silicon Surfaces for Solar Cells. *Appl. Phys. Lett.* **2006**, *88* (203107), 1−3.
(18) Nakakubo, Y.; Matsuda, A.; Fukasawa, M.; Takao, Y.; Tatsumi, T.; Eriguchi, K.; Ono, K. Optical and Electrical Characterization of Hydrogen-Plasma-Damaged Silicon Surface Structures and Its Impact on In-line Monitoring. *Jpn. J. Appl. Phys.* **2010**, *49* (08JD02), 1−6.
(19) Hook, T. B.; Adler, E.; Guarin, F.; Lukaitis, J.; Rovedo, N.; Hooke, K. S. The Effects of Fluorine on Parametrics and Reliability in a 0.18-μm 3.5/6.8 nm Dual Gate Oxide CMOS Technology. *IEEE Trans. Electron Devices* **2001**, *48*, 1346−1353.
(20) Arana, L. R.; de Mas, N.; Schmidt, R.; Franz, A. J.; Schmidt, M. A.; Jensen, K. F. Isotropic Etching of Silicon in Fluorine Gas for MEMS Micromachining. *J. Micromech. Microeng.* **2007**, *17*, 384−392.
(21) Tajima, S.; Hayashi, T.; Ishikawa, K.; Sekine, M.; Hori, M. Evaluation of Gas-Surface Reaction Dynamics during the Plasmaless Si Etching using NO/F_2 Gas Mixture. *Proceedings of the 34th International Symposium on Dry Process*, **2012**, Tokyo, Japan, November 15, p 25.
(22) Lieberman, M. A.; Lichtenberg, A. J. *Principles of Plasma Discharges and Materials Processing*, 2nd ed.; John Wiley & Sons, Inc.: Hoboken, NJ, 2005; p 573.
(23) Tougaard, S.; Jørgensen, B. Absolute Background Determination in XPS. *Surf. Inter. Anal.* **1985**, *18*, 17−21.
(24) Wagner, C. D.; Davis, L. E.; Zeller, M. V.; Taylor, J. A.; Raymond, R. H.; Gale, L. H. Empirical Atomic Sensitivity Factors for Quantitative Analysis by Electron Spectroscopy for Chemical Analysis. *Surf. Interface Anal.* **1981**, *3*, 211−225.
(25) Moulder, J. F.; Stickle, W. F.; Sobol, P. E.; Bomben, K. D. *Handbook of X-ray Photoelectron spectroscopy a reference book of standard spectra for identification and interpretation of XPS data*; ULVAC-PHI, Inc. and Physical Electronics USA, Inc.: Chanhassen, MI, 1995; pp 25 and 252.
(26) Yanai, T.; Tew, D. P.; Handy, N. C. A New Hybrid Exchange-Correlation Functional using the Coulomb-Attenuating Method (CAM-B3LYP). *Chem. Phys. Lett.* **2004**, *393*, 51−57.
(27) Bean, K. E. Anisotropic Etching of Silicon. *IEEE Trans. Electron. Dev.* **1978**, *25*, 1185−1193.
(28) Hefty, R. C.; Holt, J. R.; Tate, M. R.; Ceyer, S. T. Atom Abstraction and Gas Phase Dissociation in the Interaction of XeF_2 with Si(100). *J. Chem. Phys.* **2008**, *129* (214701), 1−14.
(29) Flamm, D. L. Mechanisms of Silicon Etching in Fluorine- and Chlorine-Containing Plasmas. *Pure Appl. Chem.* **1990**, *62*, 1709−1720.
(30) Watanabe, H.; Hosoi, T. *Fundamental Aspects of silicon carbide oxidation in "Physics and Technology of Silicon Carbide Devices*; Hijikata, Y., Ed.; InTech: New York, 2012; p 238.
(31) Clark, D. T. In *Photon, Electron and Ion Probes of Polymer Structure and Properties*; Dwight, D. W., Fabish, T. J., Thomas, H. R., Eds.; American Chemical Society: Washington, D.C., 1981; pp 247−291.
(32) Horie, M. Plasma-Structure Dependence of the Growth Mechanism of Plasma-Polymerized Fluorocarbon Films with Residual Radicals. *J. Vac. Sci. Technol., A* **1995**, *13*, 2490−2497.
(33) Pereira, J.; Pichon, L. E.; Dussart, R.; Cardinaud, C.; Duluard, C. Y.; Oubensaid, E. H.; Lefaucheux, P.; Boufnichel, M.; Ranson, P. In situ X-ray Photoelectron Spectroscopy Analysis of SiO_xF_y Passivation Layer Obtained in a SF_6/O_2 Cryoetching Process. *Appl. Phys. Lett.* **2009**, *94* (071501), 1−3.
(34) Bashouti, M. Y.; Pietsch, M.; Sardashti, K.; Brönstrup, G.; Schmitt, S. W.; Srivastava, S. K.;, Ristein, J.; Arbiol, J.; Haick, H.; Christiansen, S. *Hybrid Silicon Nanowires: From Basic Research to Applied Nanotechnology in "Nanowires - Recent Advances"*; Peng, X., Ed.; InTech: New York, NY, 2012; p 186.
(35) Diniz, J. A.; Tatsch, P. J.; Pudenzi, M. A. A. Oxynitride Films Formed by Low energy NO^+ Implantation into Silicon. *Appl. Phys. Lett.* **1996**, *69*, 2214−2215.
(36) Kim, Y.-H.; Hwang, M. S.; Kim, H. J.; Kim, J. Y.; Lee, Y. Infrared Spectroscopy Study of Low-Dielectric-Constant Fluorine-Incorporated and Carbon-Incorporated Silicon Oxide Films. *J. Appl. Phys.* **2001**, *90*, 3367−3370.
(37) San Andrés, E.; del Prado, A.; Martínez, F. L.; Mártil, I.; Bravo, D.; Lopéz, F. J. Rapid Thermal Annealing Effects on the Structural Properties and Density of Defects in SiO_2 and SiN_x:H Films Deposited by Electron Cyclotron Resonance. *J. Appl. Phys.* **2000**, *87*, 1187−1192.
(38) Pandey, R. K.; Patil, L. S.; Bange, J. P.; Patil, D. R.; Mahajan, A. M.; Patil, D. S.; Gautam, D. K. Growth and Characterization of SiON Thin Films by using Thermal-CVD Machine. *Opt. Mater.* **2004**, *25*, 1−7.
(39) Dupuis, J.; Fourmond, E.; Lelièvre, J. F.; Ballutaud, D.; Lemiti, M. Impact of PECVD SiON Stoichiometry and Post-Annealing on the Silicon Surface Passivation. *Thin Solid Films* **2008**, *516*, 6954−6958.
(40) Criado, D.; Pereyra, I.; Alayo, M. I. Study of Nitrogen-Rich Silicon Oxynitride Films Obtained by PECVD. *Mater. Charact.* **2003**, *50*, 167−171.
(41) Bentrup, U.; Brückner, A.; Richter, M.; Fricke, R. NO_x adsorption on MnO_2/NaY Composite: an In situ FTIR and EPR Study. *Appl. Catal. B: Environ.* **2001**, *3* (2), 229−241.
(42) Hefty, R. C.; Holt, J. R.; Tate, M. R.; Ceyer, S. T. Mechanism and Dynamics of the Reaction of XeF_2 with Fluorinated Si(100): Possible Role of Gas Phase Dissociation of a Surface Reaction Product in Plasmaless Etching. *J. Chem. Phys.* **2009**, *130* (164714), 1−13.
(43) Tate, M. R.; Gosalvez-Blanco, D.; Pullman, D. P.; Tsekouras, A. A.; Li, Y. L.; Yang, J. J.; Laughlin, K. B.; Eckman, S. C.; Bertino, M. F.; Ceyer, S. T. Fluorine Atom Abstraction by Si(100). I. Experimental. *J. Chem. Phys.* **1999**, *111*, 3679−3696.
(44) Li, Y. L.; Pullman, D. P.; Tsekouras, A. A.; Gosalvez, D. B.; Laughlin, K. B.; Zhang, Z.; Schulberg, M. T.; Gladstone, D. J.; McGonigal, M.; Ceyer, S. T. Experimental Verification of a New Mechanism for Dissociative Chemisorption: Atom Abstraction. *Phys. Rev. Lett.* **1995**, *74*, 2603−2606.

(45) Yeh, C.-F.; Chen, C.-L.; Lin, G.-H. The Physicochemical Properties and Growth Mechanism of Oxide (SiO_{2-x} F_x) by Liquid Phase Deposition with H_2O Addition Only. *J. Electrochem. Soc.* **1994**, *141*, 3177−3181.
(46) Safety data sheet of fluosilicic acid, Sigma-Aldrich-01302 1−7.
(47) Kim, H. M.; Shibuya, M.; Yoshida, A.; Kitagawa, M. Gas-Phase Etching with ClF_3 Gas at Atmospheric Pressure and at Room Temperature − Anisotropic Etching. *Appl. Surf. Sci.* **1998**, *133*, 1−4.